GRS 1915+105 : High-energy Insights with *SPI/INTEGRAL*

Robert Droulans[*]

Université de Toulouse ; UPS ; CESR ; 9 avenue du Colonel Roche, F-31028 Toulouse Cedex 9, France
CNRS ; UMR5187 ; F-31028 Toulouse, France
E-mail: `Robert.Droulans@cesr.fr`

Elisabeth Jourdain

Université de Toulouse ; UPS ; CESR ; 9 avenue du Colonel Roche, F-31028 Toulouse Cedex 9, France
CNRS ; UMR5187 ; F-31028 Toulouse, France

We report on results of two years of INTEGRAL/SPI monitoring of the Galactic microquasar GRS 1915+105. From July 2004 to May 2006, the source has been observed twenty times with long (∼100 ks) exposures. We present an analysis of the SPI data and focus on the description of the high-energy (> 20 keV) output of the source. We found that the $20-500$ keV spectral emission of GRS 1915+105 was bound between two states. It seems that these high-energy states are not correlated with the temporal behavior of the source, suggesting that there is no direct link between the macroscopic characteristics of the coronal plasma and the the variability of the accretion flow. All spectra are well fitted by a thermal Comptonization component plus an extra high-energy powerlaw. This confirms the presence of thermal and non-thermal electrons around the black hole.

7th INTEGRAL Workshop
September 8-11 2008
Copenhagen, Denmark

---

[*]Speaker.

1. Introduction

GRS 1915+105 is among the most notorious accreting black holes in our Galaxy. Not only is it one of the brightest and most variable X-ray sources in the sky (see Castro-Tirado et al. 1992 for a first detection report and Belloni et al. 2000 for detailed variability analysis), but it is also the first Galactic object in which superluminal plasma ejections have been observed (Mirabel & Rodriguez 1994). Consequently, much work has been done to try to understand the complex nature of the accretion flow (see e.g. the comprehensive analysis by Done, Wardziński & Gierliński 2004) and the disk-jet coupling in this binary system. An extensive review on these aspects can be found in Fender & Belloni (2004). Very recently, Rodriguez et al. (2008a & 2008b) presented an extended report on GRS 1915+105 discussing insights gained from a 2-year long monitoring campaign involving multi-wavelength observations.

However, most of the recent studies focus on the astonishing X-ray properties, the soft γ-ray emission (> 100 keV) being generally observed at poor signal to noise ratio. Understanding the high-energy behavior of the source is nevertheless very important as it is assumed to trace the physical processes occurring at the innermost regions surrounding the black-hole (e.g. Galeev et al. 1979 or Malzac 2007 for a review). Featuring good spectral resolution and sensitivity up to several MeV, SPI is a good instrument to tackle this issue.

The emission ranging from hundreds of eV up to almost $1\,MeV$ is generally assumed to originate from two components (e.g. Vilhu et al 2001). While the softer part is unanimously attributed to thermal emission from the disk, various interpretations exist concerning the origin of the high-energy emission. Detailed analysis of joint RXTE/OSSE observations allowed Zdziarski et al. (2001 & 2005) to rule out some of these interpretations. They suggested that the observed $10-500\,keV$ emission originated from inverse Compton scattering of the soft disk photons by a hybrid thermal/non-thermal electron population.

Here we present all SPI observations of GRS 1915+105 from July 2004 to May 2006 (Droulans & Jourdain 2009). We focus on gaining the most accurate high-energy picture of the source, mainly through extensive spectral analysis. First we briefly describe the instrument as well as our data reduction methods. The observational results are presented and further discussed in the concluding part of the document.

2. Observations and data reduction

2.1 INTEGRAL/SPI

SPI is a high resolution γ-ray spectrometer (Vedrenne et al. 2003) aboard the INTEGRAL observatory. The observational strategy of the INTEGRAL mission is based on approximately 3-day long revolutions during which one or several fields of view are sampled by means of $30-40$ minute long fixed pointings, separated by a $2°$ angular distance. As the number of SPI pixels is small (among the initial 19 detectors, two broke down reducing the detector plane to only 17 pixels), this so-called 'dithering' scheme (see Jensen et al. 2003 for details) is essential for SPI image reconstruction. In particular, combining the data from a set of dithered pointings allows one to enhance the precision of flux extraction (see e.g. Joinet et al. 2005).

2.2 Data analysis

Obs ID	MJD start	MJD stop	Exp time $_{(s)}$	$<F>_{(mCrab)}$	Γ	$\chi^2/27$
231	53253.20	53253.95	48412.50	322.5 ± 5.0	2.80 ± 0.06	0.97
242	53285.10	53285.75	42782.20	259.5 ± 4.5	3.09 ± 0.06	0.56
243	53288.63	53289.44	49962.72	199.8 ± 4.4	2.99 ± 0.10	1.08
246	53296.35	53297.53	77174.90	305.8 ± 3.1	3.02 ± 0.05	1.37
248	53302.88	53304.90	134148.88	201.3 ± 2.7	3.07 ± 0.07	0.84
250	53309.14	53310.22	72648.77	199.1 ± 3.9	3.10 ± 0.10	0.71
251	53311.32	53312.77	84373.42	320.4 ± 3.9	3.00 ± 0.06	1.12
255	53324.27	53325.46	81422.62	152.1 ± 3.0	2.85 ± 0.09	0.64
295	53442.95	53444.15	85681.48	255.5 ± 2.8	3.47 ± 0.07	1.40
305	53472.66	53475.66	91334.75	180.2 ± 2.7	3.52 ± 0.08	0.96
315	53503.53	53504.55	69072.34	158.3 ± 3.4	3.00 ± 0.10	1.26
361	53640.92	53641.58	70136.04	123.2 ± 3.1	3.24 ± 0.13	0.92
366	53655.52	53657.87	161541.02	169.7 ± 3.0	3.47 ± 0.09	1.46
367	53659.23	53660.83	109687.94	160.4 ± 3.6	3.48 ± 0.11	1.41
368	53661.51	53663.78	154549.29	187.2 ± 2.8	3.42 ± 0.07	1.68
369	53664.31	53665.53	52753.31	194.0 ± 6.4	3.43 ± 0.14	1.06
373	53676.27	53677.43	83798.38	87.2 ± 3.8	3.14 ± 0.18	1.07
379	53694.27	53695.47	90421.32	183.1 ± 3.9	3.08 ± 0.10	0.89
423	53825.88	53828.23	119129.04	391.1 ± 4.2	2.80 ± 0.04	3.07
431	53851.94	53852.20	15509.04	278.7 ± 7.2	2.80 ± 0.10	1.46

Table 1: Log of the SPI observations along with average flux, photon index and χ^2/ν from a simple powerlaw model fit.

We analysed all public data from nearly two years of SPI observations on GRS 1915+105 (July 2004 – May 2006). For each revolution, we first gathered all pointings where GRS 1915+105 was less than 12° off the central axis. Pointings showing contamination by solar flares or radiation belt exit/entry were excluded. The log of the resulting $1.7\,Ms$ of observational coverage is given in Table 1. In order to detect the emitting sources in the field of view, we used the SPIROS software (Skinner & Connell 2003) to produce $20-50\,keV$ images for each observation. The positions of the active sources (detected at a minimum of 5σ) were then given as input to a specific flux-extraction algorithm, using the SPI instrument response for sky-model fitting. From there we started to analyse the background and source behavior for each observation. We first allowed the background pattern as well as the main source(s) to vary between successive pointings. In this way we determine each component's most appropriate variability timescale for the final data reduction. We used pointing-durations ($\approx 2\,ks$) as a timescale for the GRS 1915+105 light-curves and adapted the time sampling for subsequent extraction of the $20\,keV-8\,MeV$ spectra according to the observed temporal behavior. This method allowed us to minimize the error bars without losing any scientific information.
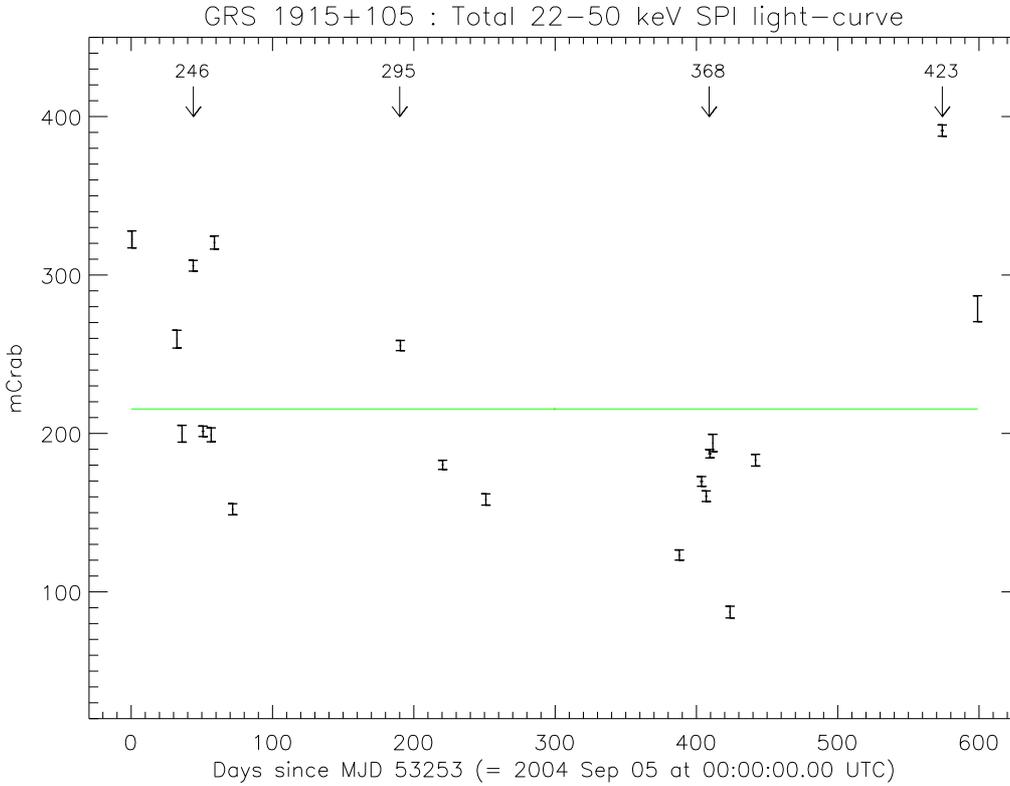
3. Results

3.1 Light-curves

Figure 1: Mean 22-50 keV flux per observation from September 2004 to May 2006

Figure 1 displays the total $20 - 50\,keV$ light-curve for our observational period. GRS 1915+105 shows relevant long-term variability, the averaged source flux per observation ($\approx$ one-day) spans between 90 and $380\,mCrab$, with approximate uncertainty of $5\,mCrab$. On the shorter science-window timescale ($\approx 2\,ks$), the obtained individual light-curves show in general lower variability. Within a single observation, the source flux varies by at most a factor of 2. As GRS 1915+105 is well known for being very variable in X-rays, we also considered SPI-simultaneous $1.2 - 12$ keV ASM light-curves to compare the X- and soft γ-ray behavior of the source. We found an anti-correlation trend between the $\sim$ one-day averaged $1.2 - 12$ and $20 - 50\,keV$ source fluxes (see Figure 2 left) with a linear correlation factor ρ of -0.59 ± 0.02 and a 99% significance. On the science-window timescale however, a positive flux-correlation is discernible for some observations in which the source exhibits rather strong variability e.g. as shown in Figure 4. The variability amplitudes (parameterized by fractional rms) are not straightforward to compare since the time bins are very different between the two instruments. More importantly, the 1σ SPI errors for the individual light-curves are of the same order of magnitude than absolute rms variability, thus limiting a solid scientific interpretation.

4

3.1.1 Spectral analysis

We used XSPEC 11.3.2 (Arnaud 1996) for spectral analysis. First, each observation-averaged spectrum was fitted with a basic powerlaw model which gives a good description of most of the data. Then we characterized the spectra by flux and best-fit photon index, the latter being found to range from 2.8 to 3.5. The results are summarized in Table 1 and illustrated by a photon index versus flux diagram given in Figure 2 right. We used this figure to select four observations which will be presented in more detail in the following subsections. We selected the observations made during INTEGRAL revolutions 295 and 423 since they both have rather high average fluxes (and therefore good signal to noise ratios), but at the same time very different spectral shapes. Further, the light-curves showed no significant variability during these observations (neither in the $20-50\,keV$ band nor in X-rays), hence allowing a meaningful analysis of the observation-averaged spectrum. In addition, we selected two other observations (Rev. 246 and 368) because they were part of large multi-wavelength campaigns, allowing us to put the SPI data in a broader context.
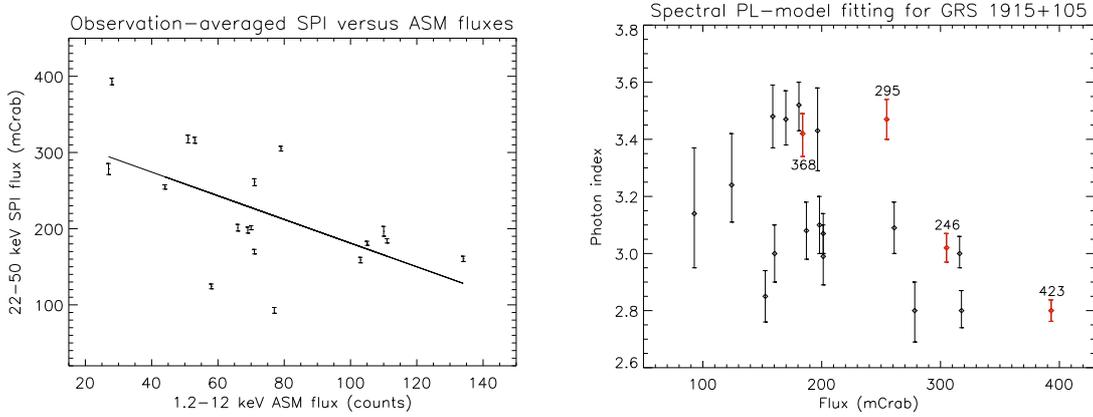

Figure 2: Left : One day timescale flux-flux relation between the $1.2-12$ and $20-50\,keV$ bands. We observe an anticorrelation in the flux trend between the two bands. **Right** : Basic source characteristics : model photon index versus mean 22-50 keV flux per observation. The observations that are discussed in the text are highlighted in red.

3.1.2 Observations 295 and 423

From the ASM light-curves in Figure 3, we see that during both observations GRS 1915+105 showed very similar X-ray activity, characterized by low flux and almost no variability. The temporal properties in the $20-50\,keV$ band are also quite similar, with again little variability during both observations. On the other hand, spectral characteristics are found to be significantly different, with photon indices of of 3.47 ± 0.07 and 2.80 ± 0.04 respectively. We then investigated these differences through more detailed spectral modelling. From Table 1 one can see that the simple powerlaw model gives a rather poor fit for observation 295. More precisely, we noticed that above $100\,keV$ all spectral points are located above the fitted powerlaw. Pure thermal Comptonization models like COMPTT (where the Comptonized spectrum is completely determined by the plasma temperature and its optical depth, Titarchuk 1994) can thus be ruled out ($\chi^2/\nu = 72/26$, see Table 2). Assuming
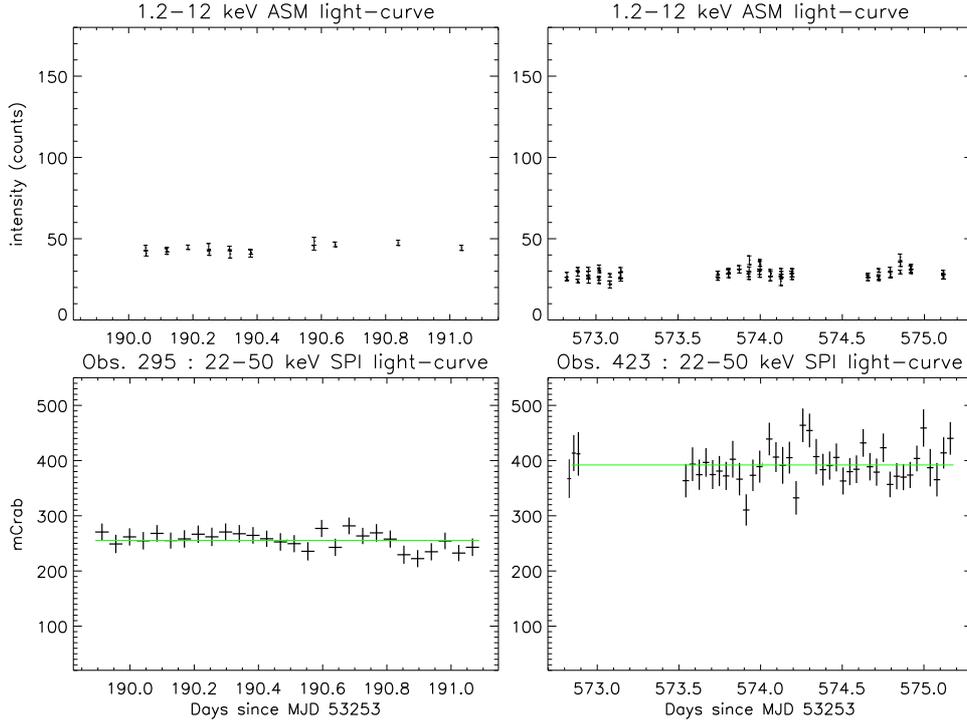
Figure 3: ASM and SPI light-curves for observations 295 and 423. For both observations the source exhibits low flux and very little variability in the ASM band. In the $20-50\,keV$ SPI band we observe similar stability during both observations with intermediate and high flux respectively.

that the low-energy part is nonetheless produced through thermal Comptonization, one needs to add a further spectral component. We thus chose to add a powerlaw as a phenomenological description of the observed high-energy tail. Given the error amplitude above $100\,keV$, we arbitrarily fixed the photon index to 2.0. The resulting fit ($kT_e = 16.3^{+1.2}_{-0.9}\,keV$ and $\tau = 0.57$[1]) is in very good agreement with our data ($\chi^2/\nu = 17/25$) and the *F-TEST* indicates a probability of $\sim 10^{-9}$ that this improvement has been a chance event. As a last step we applied the Poutanen & Svensson (1996) COMPPS model which describes Comptonization from a hybrid thermal/non-thermal electron plasma. This iterative scattering method assumes a powerlaw distribution ($\propto \gamma^{-\Gamma_e}$) up to a Lorentz factor γ_{min} below which the plasma thermalizes to a Maxwellian distribution. We fixed a spherical geometry and assumed the reflection component to be insignificant, enabling a straightforward comparison with COMPTT+PL. Note that COMPPS poses more constraints than COMPTT+PL, as it requires both components (thermal and non-thermal) to be linked, whereas the former does not. Equally good fitting results ($\chi^2/\nu = 17/25$) for both models indicate that the observed $20-500\,keV$ emission is most likely to originate from thermal and non-thermal Comptonization processes.

For observation 423, the basic powerlaw fit is clearly unacceptable ($\chi^2/\nu = 83/27$) due to the marked curvature around $50\,keV$, leaving clear evidence for thermal processes. Replacing the powerlaw by a pure thermal component improved the fit and gave $\chi^2/\nu = 42/26$. However, this interpretation is not able to account for the observed emission above $200\,keV$, again suggesting the presence

---

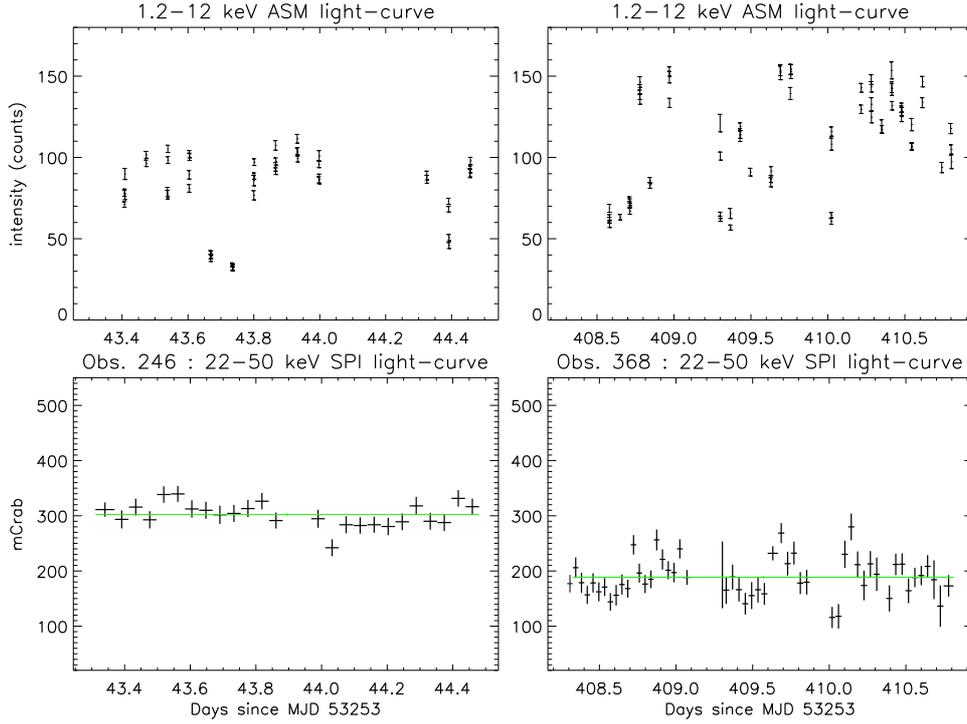[1]fixed to its best-fit value for error calculation on kT_e

Figure 4: ASM and SPI light-curves for observations 246 and 368. During the latter a correlation (on a $\approx 2\,ks$ timescale) between the $1.2-12$ and $20-50\,keV$ bands is noticeable, hinting that both bands are tracing the evolution of the Comptonized emission.

of an additional component. We thus keep the hybrid Comptonization models ($\chi^2/\nu = 37/25$ for COMPTT+PL and $\chi^2/\nu = 37/24$ for COMPPS) as our preferred description for observation 423.

The relevant fitting results are summarized in Table 2 and discussed in section 4.

3.2 Observations 246 and 368

Both observations have already been intensively studied. Observation 246 is discussed by Rodriguez et al. (2008b) who conducted detailed spectro-temporal analysis by means of multi-wavelength coverage. They found that the source showed periodic X-ray cycles, identified as alternations of ν and ρ classes (see Belloni et al. 2000 for definitions). INTEGRAL observation 368 was again part of a large multi-wavelength campaign, this time involving the Suzaku satellite (Ueda et al. 2006). These authors identified the observed X-ray variability pattern to be the signature of a high flux transition from a soft class χ to class θ. We find the same variability pattern in X-rays as in the $20-50\,keV$ SPI band (Figure 4), indicating that both bands are probably sampling the temporal behavior of the same component. For observation 246 there seems to be a similar correspondence, although less clear due to lower variability amplitude in the SPI band. Both spectra are fitted with thermal + non-thermal Comptonization models (COMPTT+PL and COMPPS) which provide the best agreement to the data (see Table 2). Compared to the joint JEMX/ISGRI spectrum from observation 246 (Rodriguez et al. 2008b), our SPI data are found to have almost the same spectrum than the one produced by these authors from only stable low/hard X-ray intervals (Interval I in Rodriguez et al. 2008b), whereas the very short X-ray spikes originating from the disk (Intervals
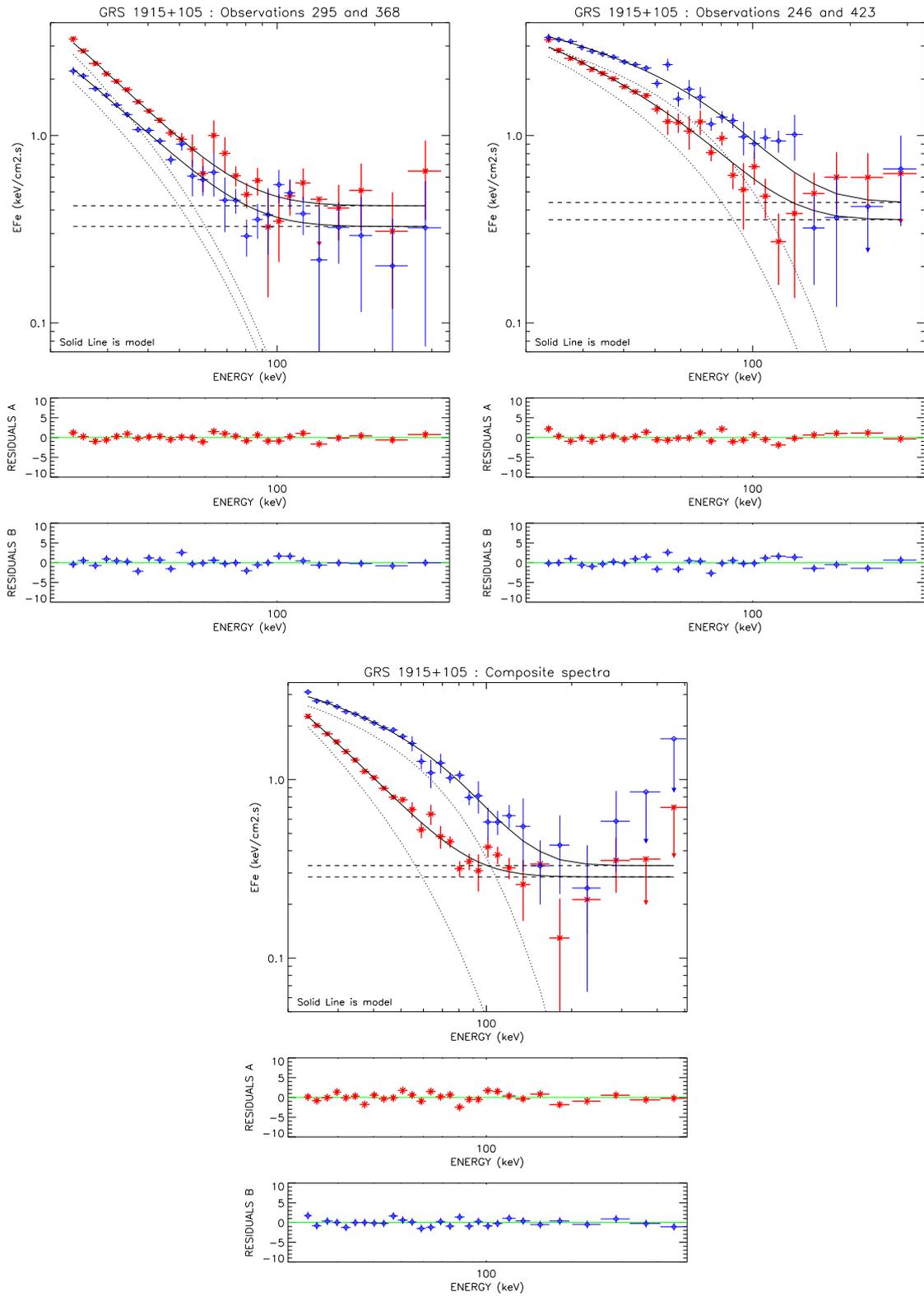
Figure 5: COMPTT+PL best fits. **Left** : Observations 295 (red stars) and 368 (blue diamonds). **Right** : Observations 246 (red stars) and 423. **Bottom** : Soft sample (red stars) and hard sample.

II and IV) are washed out. This shows that the SPI spectra of the one day averaged Comptonized emission are not influenced by any peculiar outburst-behavior on very short time-scales. Likewise, a comparison with simultaneous Suzaku observations leads to similar conclusions for observation 368.

3.3 Cross-comparison

When comparing the results of these four high-lighted observations, we notice that the X-ray variability and the spectral behavior at higher energies seem to be completely uncorrelated. Except for a slight difference in flux, the SPI spectra from observations 368 and 295 (illustrated in Figure 5 left) show the same characteristics, whereas the temporal behavior in X-rays is seen to be dramatically different (compare Figure 3 left and Figure 4 right). A similar high-energy correspondence can be observed between observations 246 and 423 (Figure 5 right), although again no similarities are found in X-rays. We thus see that for similar X-ray variability, the $20 - 500 \, keV$ spectra can be different and reciprocally that for similar ($\sim$ one day averaged) high-energy spectral behavior, the source may exhibit very unlike $1.2 - 12 \, keV$ activity.

3.4 Composite spectra

In order to further investigate the high-energy tail of GRS 1915+105, we decided to group data from observations with similar spectra. Improved statistics should allow us to put better constraints on the parameters of the fitted models. Hence, we isolated two opposite groups in the spectral index versus flux diagram (Figure 2 right) for which we generated composite spectra. The first group is characterized by a rather low $20 - 50 \, keV$ flux ($\sim 200 \, mCrab$) and a very soft spectral shape ($\Gamma \approx 3.45$); hereafter we will call it the *soft sample*. The second group on the other hand has hard colors ($\Gamma \approx 2.90$) and high average flux ($\sim 330 \, mCrab$) in the $20 - 50 \, keV$ band; it will accordingly be called the *hard sample*. We note that the previously presented observations 295/368 and 246/423 are representative of each group, respectively. We observed that some observations had intermediate characteristics, well fitted by a single power law of index $\Gamma \approx 3.1$. These were excluded from the regrouped spectra in order to best describe the limiting spectral shapes at high energies. As a result, our two samples are likely to illustrate the boundary "Comptonization states" between which the source seems to be continuously switching. However, more detailed investigations (beyond the $\sim$ 1 day analysis presented here) are needed to determine the timescale of this spectral evolution.

We fitted both composite spectra shown in Figure 5 (bottom) with several models and summarize the results in Table 2. Each time the thermal + non-thermal Comptonization models gave the best fit to the data and demonstrated the need for an additional high-energy component (see *F-TEST* values in Table 2). The composite spectral analysis thus confirms the previously outlined interpretation, which will be further discussed in the next section.

4. Discussion

We interpret the $20 - 500 \, keV$ emission of GRS 1915+105 as Comptonized emission from a combination of thermal and non-thermal source processes. Given the similarities of the observed

Obs ID	kT_{bb} (keV)	COMPTT kT_e (keV)	τ	F_{comptt}	PL α	K_{pl}	χ^2/ν	FTEST
246	1.0f	$83^{+4.2}_{-2.3}$	0.08	-	-	-	32/26	
		$18.2^{+1.1}_{-1.0}$	0.97	$3.64^{+0.04}_{-0.04}$	2.0f	$3.48^{+1.05}_{-0.96}$	27/25	4×10^{-2}
295	1.5f	44	0.18	-	-	-	72/26	
		$16.3^{+1.2}_{-0.9}$	0.57	$2.73^{+0.03}_{-0.03}$	2.0f	$3.95^{+0.66}_{-0.56}$	17/25	2×10^{-9}
368	1.5f	39	0.20	-	-	-	74/26	
		$13.4^{+1.0}_{-0.9}$	0.86	$1.94^{+0.03}_{-0.03}$	2.0f	$3.28^{+0.54}_{-0.56}$	29/25	1×10^{-6}
423	1.0f	$41^{+1.2}_{-1.7}$	0.45	-	-	-	42/26	
		$19.2^{+1.0}_{-1.0}$	1.20	$4.91^{+0.05}_{-0.05}$	2.0f	$4.27^{+1.29}_{-1.38}$	37/25	8×10^{-2}
SS	1.5f	48	0.13	-	-	-	152/26	
		$16.5^{+0.6}_{-0.6}$	0.62	$2.07^{+0.03}_{-0.03}$	2.0f	$2.75^{+0.28}_{-0.29}$	31/25	3×10^{-10}
HS	1.0f	$38^{+0.9}_{-0.9}$	0.47	-	-	-	30/26	
		$17.7^{+0.7}_{-0.7}$	1.28	$4.13^{+0.04}_{-0.04}$	2.0f	$3.31^{+0.91}_{-0.95}$	19/25	8×10^{-4}

Table 2: Spectral fitting results for the high-lighted observations. For each spectrum, the first row corresponds to a simple thermal Comptonization model (COMPTT) whereas the second row contains the COMPTT + PL parameters. The seed photon temperature is fixed to $1.0\,keV$ and $1.5\,keV$ for the harder and softer spectra respectively. COMPTT errors are calculated on kT_e while fixing τ to its best fit value. F_{comptt} denotes the integrated 20-500 keV energy flux from the thermal component and is given in units of $\times10^{-9}\,erg/cm^2/s$. K_{pl} is the flux normalization at $100\,keV$ of the non-thermal power law and is given in units of $\times10^{-5}\,photons\,cm^{-2}s^{-1}keV^{-1}$

temporal properties, the ASM band is likely to sample the same emission component as the $20-50\,keV$ SPI band. This is in agreement with the results of Done, Wardziński & Gierliński (2004) who show that except for ultrashort disc-dominated X-ray spikes the accretion disc has no significant effect above $3\,keV$ (see also Rodriguez et al. 2008b). The spectra obtained during observations 295 and 368 show that for different X-ray classes (i.e. different temporal behavior of the accretion flow) the high energy spectra can be very similar. Conversely, observations 295 and 423 show that within stable emission episodes, there can be significant differences in the spectral behavior of the source. Assuming that the $3-50\,keV$ emission originates from the Comptonizing corona (see Malzac 2007 or Done et al. 2007 for details), this indicates that there is no correlation between the temporal variability and the macroscopic properties of the Comptonizing flow. As they give better statistics above $100\,keV$, we will thus use our composite spectra to further discuss both Comptonization components and put our findings in a more general context.

4.1 The soft sample

From spectral modelling we find the intersection point of the two components to be around $60\,keV$. At higher energies, the non-thermal processes dominate. Both the thermal and non-thermal components have approximately the same luminosity above $20\,keV$. If these two components orig-

inate from the same population (COMPPS results), the electrons are found to thermalize around Lorentz factor $\gamma_{min} = 1.3$. The mildly hot Compton cloud ($kT_e = 14.72 \pm 0.15\,keV$) is found to be marginally optically thick ($\tau = 2.7^{+0.10}_{-0.25}$) which is the expected configuration for black-hole binaries in the very high state (Done & Kubota 2006). We suggest that our soft composite spectrum gives a canonical high-energy representation of GRS 1915+105 in low coronal luminosity states.

4.2 The hard sample

Concerning the hard sample, the luminosity of the non-thermal component is found to be roughly the same (compatible within the errors) as for the previously discussed soft sample. However, the intersection point of the two components is now around $110\,keV$ (which corresponds to a Lorentz factor $\gamma_{min} \approx 1.39$), showing that the main difference lies in the properties of the Comptonizing thermal electrons of the corona. The plasma is found to be either hotter for similar optical depths or optically thicker for similar electron temperatures (or a mixture of both), thus enhancing the higher observed $20-50\,keV$ flux. Even though this situation cannot be completely resolved due to the observational $kT - \tau$ degeneracy, spectral fits with COMPPS indicate that it is likely that there has been a significant increase in opacity, whereas electron temperature remains between 14 and $18\,keV$. In any case, this does not affect the estimation of the total $20-500\,keV$ luminosity derived from thermal Compton scattering, which is found to be enhanced by a factor of 2 ± 0.04 in comparison with the soft sample. We interpret our spectrum as a typical representation for the high-energy emission of GRS 1915+105 in high coronal luminosity states.

5. Summary and Conclusions

We have conducted detailed high-energy spectral analysis of the microquasar GRS 1915+105 using all available SPI data from July 2004 to May 2006. We presented here our observational results on the source's high-energy output. We can summarize our findings as follows:

We found that the $\sim$ one day averaged $20-500\,keV$ spectral emission is always between two boundary states, *hard* and *soft*, which we illustrated through spectral modelling. We confirm that in the INTEGRAL-SPI data we observe no high-energy cutoff for GRS 1915+105 (Fuchs et al. 2003, Rodriguez et al. 2008b). We suggest that the high-energy cutoff from thermal Comptonization is drowned out by an additional non-thermal component. We found the non-thermal component to be statistically required in both composite samples. The spectral differences we observed in hard X-rays ($20-50\,keV$) are most likely to be coupled to the evolution of the thermal electron plasma. The bolometric luminosity calculated from the thermal component varies by a factor of 2 between soft and hard samples. In contrast, the obtained fits indicate that the non-thermal component is fairly stable. This implies that both components are not necessarily linked, i.e. they could originate from dissociated electron populations. Hence as suggested by Rodriguez et al. (2008b), the non-thermal component might be from emission from the jet. Given the length of the high-energy observations (SPI $\approx 3\,days$ or OSSE $\approx 15\,days$), it is difficult to investigate the connection between the various X-ray classes and the high-energy spectra. We pointed out that there is no direct correlation between the observed variability patterns and our $20-500\,keV$ SPI spectra. This shows that the macroscopic properties of the Comptonizing thermal electrons evolve independently from the temporal behavior of the source, i.e. independently from the fluctuations of the accretion flow. In summary, our results

give a recent high-energy picture of GRS 1915+105 and once more underline the complex nature of the accretion processes operating around this archetypal microquasar.

References

[1] Arnaud K.A., 1996, in Jacoby G.H., Barnes J., eds, ASP Conf. Ser. Vol.101, Astronomical Data Analysis Software and Systems V. Astron. Soc. Pac., San Francisco, p.17

[2] Belloni T., Klein-Wolt M., Méndez M. et al., 2000, A&A, 355, 271

[3] Castro-Tirado A.J., Brandt S. & Lund, N. 1992, IAUC, 5590, 2

[4] Done C., Wardziński G.& Gierliński M., 2004, MNRAS, 349, 393-403

[5] Done C. & Kubota A., 2006, MNRAS, 371, 1216-1230

[6] Done C., Gierliński M.& Kubota A., 2007, A&AR Volume 15, Issue 1, 1-66

[7] Droulans R. & Jourdain E., 2009, A&A, in press

[8] Fender R.P. & Belloni, T. 2004, ARA&A, 42, 317

[9] Fuchs, Y., Rodriguez J., Mirabel F. et al , 2003, A&A, 409, L35

[10] Galeev A.A., Rosner R. & Vaiana G.S. 1979, ApJ, 229, 318G

[11] Jensen P. L., Clausen K., Cassi C. et al., 2003, A&A, 411, L7

[12] Joinet A., Jourdain E., Malzac J. et al., 2005, ApJ, 629, 1008

[13] Malzac J., 2007, ApJS, 170, 175

[14] Mirabel I.F. & Rodríguez L.F., 1994, Nature, 371, 46

[15] Poutanen J. & Svensson R., 1996, ApJ, 470, 249

[16] Rodriguez J., Shaw S.E., Hannikainen D.C. et al., 2008a, ApJ, 675, 1436R

[17] Rodriguez J., Shaw S.E., Hannikainen D.C. et al., 2008b, ApJ, 675, 1449R

[18] Skinner G. & Connell P., 2003, A&A, 411, L123

[19] Titarchuk L., 1994, ApJ, 434, 313

[20] Ueda Y., Ishioka R., Sekiguchi K. et al., 2006 in "Proceedings of the VI Microquasar Workshop: Microquasars and Beyond" PoS(MQW6) 023

[21] Vedrenne G., Roques J.P, Schönfelder et al., 2003, A&A, 411, L63

[22] Vilhu O., Poutanen J., Nikula P. et al., ApJ, 553, L51

[23] Zdziarski A.A., Gierliński M., Rao A.R. et al., 2005, MNRAS 360, 825-838

[24] Zdziarski A.A., Grove J. E., Poutanen J. et al., 2000, ApJ 554 L45